Evaluation of the potential of high index Chalcogenide lenses for automotive application

Guillaume Druart, Valentin Reux, Laurent Calvez, Xianghua Zhang, Florence de La Barrière, Jean-Baptiste Volatier, Elodie Tartas, Raphael Proux

Evaluation of the potential of high index Chalcogenide lenses for automotive application

Guillaume Druart*[a], Valentin Reux[b], Laurent Calvez[b], Xiang-Hua Zhang[b], Florence De La Barrière[a], Jean-Baptiste Volatier[a], Elodie Tartas[c], Raphael Proux[d].

[a]ONERA, Chemin de la Hunière, 91761 Palaiseau Cedex, France; [b]Univ. Rennes, CNRS, ISCR (Institut des Sciences Chimiques de Rennes) – UMR 6226, F-3500 Rennes, France; [c]LYNRED, route de Valence, 38113 Veurey-Voroise, France; [d]UMICORE, ZA du Boulais, 35690 Acigné, France.

* Corresponding author: guillaume.druart@onera.fr

ABSTRACT

Infrared cameras could serve automotive applications by delivering breakthrough perception systems for both in-cabin passengers monitoring and car surrounding. However, low-cost and high-throughput manufacturing methods are essential to sustain the growth in thermal imaging markets for automotive applications, and for other close-to-consumer applications, which have a fast growth potential. With the reduction of the pixel pitch of microbolometer detectors, their cost has decreased considerably and now the optical part represents a significant part of the system cost. Fast low cost infrared lenses suitable for microbolometers are already sold by companies like Umicore, Lightpath, FLIR… Chalcogenide glasses are widely used as materials for optics because they have many cost advantages, especially due to the possibility of mass molding the optics. However, with the reduction of the pixel pitch, it is more and more difficult to design high performance lenses with a limited number of optics. The possibility of molding the optics allows us to use many highly aspherical surfaces at affordable costs. However, Chalcogenide glasses have usually a lower refractive index than other more expensive infrared materials such as Germanium. Indeed, high refractive index materials are known to be effective in attenuating the amplitude of many geometric aberrations. In this presentation, we evaluate the interest of high index Chalcogenide lenses, especially TGG and TGS, to design optical systems meeting the needs of the automobile with a limited number of optics. TGG glass has an index of refraction of 3.396 at a wavelength of 10µm, i.e. its index of refraction is close to the Silicon one and was initially studied for space applications. TGS has a lower index of refraction (3.12@10µm) but can be used in a cost effective manufacturing process by using flash spark plasma sintering (SPS) on raw powder. Demonstrators with TGG glass have been made and their performance evaluated.

Keywords: Infrared, Microbolometers, Chalcogenide, Automotive Application, Curved Sensor

1. INTRODUCTION

With the emergence of new forms of personal mobility, the automotive industry is facing a drastic change. Photonic technology, one of the six Key Enabling Technology (KET) recognized by the European Commission, plays a crucial role in meeting automotive needs and expectations. Even if all sensors are combined, limitations in the fields of assistance and autonomous vehicle are still expected. Whether they are using their own vehicle or sharing one, drivers will demand a better driving experience for themselves, their passengers and other road users: quality and safety, simplified driving (i.e. increasingly autonomous and connected cars), air quality, and combating global warming. Innovation and technology are crucial drivers for these changes: today, innovation in the automotive sector must meet higher expectations in terms of consumer and user quality of life. Photonic technologies can play a crucial role in meeting these needs and expectations. Implementation of photonic technologies in the automotive industry aims at integrating technologies in the car as well as at improving optics manufacturing methods. The new ways of driving and using a vehicle as expected in the scope of Smart Mobility ask for reliable, affordable and versatile perception systems. It is now clear that the interaction between the vehicles and environment (in and out of cabin) has to be improved. This need is even more important in the case of autonomous driving for which the four mandatory steps (starting with “hands on” and ending with “hands off”, “eyes off”

and “minds off”) are full of technical hurdles, barriers, obstacles. Depending on the level of automation (from “hands on” to “mind off”), the decisions taken by the human driver or by the autonomous vehicle change. The required reaction time by the human driver to take over the vehicle control increases with the level of automation. In other words, safe machine-human interaction requires safe perception of the environment and the human driver state inside the vehicle. Traditionally, two major complementary approaches exist to perform perception. Object based approaches relays on the identification of objects on vehicle environment. In complement, map fusion approaches perform perception based on building map models of the environment. Traditionally, these two complementary approaches are conceived and adapted to better fit specific sensors. For instance, visible image sensors are well fitted to perform object perception while map fusion perception work well with LIDAR and RADAR sensors.

Infrared cameras, taking benefits of Long Wave Infra-Red bandwidth (LWIR) in which all object radiates energy depending only on its structure and temperature, could deliver breakthrough perception systems thanks to their unique feature over visible or Near Infra-Red (NIR) cameras. Therefore, they could be a key technology for autonomous vehicles by making them safer and will improve object classification of the automotive sensor suite in all light conditions, provide redundancy and thus extend vehicle autonomy towards level 3 and beyond, operating 24/7. Infrared cameras could be a must-have in the mix of sensing systems since the driver and passenger monitoring needs to be improved as well as the environment surrounding monitoring, in all light and weather conditions:

- The facial thermal imaging, combined to computational psychophysiology, will dramatically improve the monitoring of the driver on vital signs including liveliness, drowsiness, and emotions. The same systems will also contribute to the overall monitoring of the vehicle interior for comfort management. The combination of the two monitoring capabilities enables individualization of the vehicle, with an instantaneously adaptation to all functions and services of such a vehicle to the user and passengers.
- Environment recognition as an out-of cabin application essential feature will also benefit from the addition of the LWIR thermal sensing to existing systems composed of LIDAR, RADAR and other vision systems. In addition to those, thermal perception is the only technology that is accurate and reliable in all light and weather conditions, even in extreme cases.

An IR thermal module is based on an uncooled InfraRed Focal Plane Array (IR FPA) based on a microbolometer technology, an optical system focusing in order to provide a thermal infrared image, an embedded system dedicated to the correction of the raw IR image. However, to meet the cost and performance requirements of automotive industry, the whole system needs to aggregate different cutting-edge technologies, for which technological developments are required. First, the primary cost is the microbolometer whose technologies are developed to reduce the sensor size and pixel pitch like detectors for cell phones. In 2012, DARPA founded three contracts to develop sub $500 thermal imaging camera with 12 µm pixels. At the same time, LYNRED with CEA released IR FPAs with 12µm pixel pitch [1]. Nowadays, IR FPAs with 10µm pixel pitch can be found [2]. Infrared cameras as smartphone add-ons released by FLIR (FLIRONE camera) or SEEKTHERMAL can be considered as the first consumer market for thermal imaging that reaches prices under $250. Indeed this step change in volumes enables a step change in system costs and now thermal imaging can move into automotive applications [3][4][5]. Both thermal add-ons use 12µm pixel pitch technology. Now the optics represents a non-negligible part of the cost. Chalcogenide glasses represent a cost effective alternative to single-crystalline Germanium or poly-chrystalline ZnSe. Moreover, these IR glasses have good material’s thermo-optic properties.

The aim of this paper is to evaluate high refractive index Chalcogenide glass to design a low cost and high performance infrared lens that will detect LWIR light both for in-cabin passengers monitoring and for car surrounding. In a first part, two high refractive index Chalcogenide glass are presented: TGG and TGS. They have an index of refraction greater than 3. In a second part, we study the impact of using TGG for two designs and with field of views of interest for automotive application. A special focus is made on the correction of the field curvature. The study is done with a VGA (640x480 pixels) detector with a pixel pitch of 10µm. Finally, a status on the manufacturing of TGG lenses in the framework of Heliaus project is presented.

2. STUDY OF HIGH-INDEX CHALCOGENIDE GLASS FOR VGA SENSORS

Chalcogenide glasses are good candidates to make low cost IR optics. The fact that these Chalcogenide glasses can be molded further reduces the cost of the optics. Nowadays, the most common IR lenses available on the market are based on As_2Se_3 (n=2.81@1.5µm [6]) and Ge-As-Se glasses (n=2.75@10µm [7]). Glass compositions free of Germanium such as As_2Se_3 are low-cost and attract a growing interest even if they present weaker mechanical properties. However, the final cost of IR optics, especially small-size optics, is mainly governed by the synthesis and processing instead of raw materials. This problem particularly concerns the automotive industry which seeks to take advantage of the reduction of the size of the detectors and the reduction of the size of the optics (now around 8mm). Therefore, Chalcogenide glasses with higher index of refraction could be very interesting as long as they lead to a reduction of the number of lenses in a design. Indeed higher index of refraction will lead to high optical power and reduced geometric aberrations. Table 1 lists some glass compositions having high refractive index with their characteristic temperatures (Tg is the Glass-transition temperature and Tx is the crystallization temperature).

Table 1. Composition and properties of some chalcogenide glasses with high refractive index

Composition	n @wavelength	Tg(°C)	Tx(°C)	Ref.
$Ga_{10}Ge_{15}Te_{75}$	3.39@10µm	172	285	[8]
$Ge_{20}Se_2Te_{78}$	~3.42@10µm	153	250	[9],[10]
$Ge_{20}Se_{10}Te_{70}$	~3.26@10µm	156	236	[9],[10]
$Ge_{20}Se_{60}Te_{20}$	~2.55@10µm	188	405	[9],[11]
$Ge_{20}Se_{70}Te_{10}$	~2.50@10µm	175	430	[9],[11]
$Ge_{25}Se_{10}Te_{65}$	3.12@10µm	189	340	[11],[12]

For industrial applications, ideal composition should present a high refractive index, a glass transition temperature ideally above 180°C and a good thermal stability (highest difference of temperature between Tx and Tg) in order to be easily shaped. Within the framework of the Heliaus project, we focus on two types of glass composition: $Ga_{10}Ge_{15}Te_{75}$ called in the following TGG and $Ge_{25}Se_{10}Te_{65}$ called in the following TGS.

TGG has a high index of refraction close to that of Silicon, despite having a transition temperature slightly lower than 180°C. It was fabricated by the University of Rennes for space application [8]. Tellurium based glasses are the only known vitreous materials with good chemical and thermal stability as well as low losses in the 6-20µm spectral range. In the framework of the Heliaus project, we decided to make lenses in TGG by diamond manufacturing technics.

TGS has a lower index of refraction than TGG but still greater than a value of 3. It has however a better transition temperature and a better thermal stability. Moreover, this glass is compatible with spark plasma sintering (SPS) to mold lenses in a potential lower cost than traditional molding technics. Indeed, usually, glass ingots of big diameter (around 20cm) are produced in high volume and discs are obtained by first coring and then cutting. In the next step, glass slices are molded above Tg to final shape for making high precision IR optics. The coring process could induce a material loss higher than 30%, which can only partially be re-used as starting material. In this context, developing a process that allows for making a near-shape or even finished IR optics by using residual glass may be of high interest. In Ref [13], Univ. of Rennes demonstrated that flash SPS sintering gives the possibility to shape lenses from raw powder rapidly and reproducibly.

The refractive index of TGG and TGS are given in Fig.1.

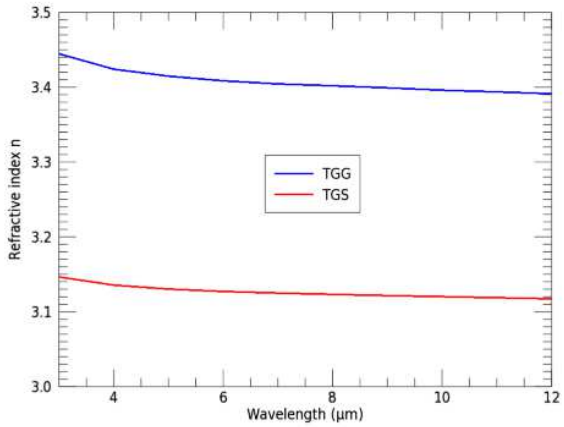

Figure 1. Refractive index of TGG and TGS.

3. DESIGN STUDY WITH HIGH-INDEX CHALCOGENIDE GLASS FOR VGA SENSORS

The current trend is to reduce the size of the pixels and therefore the size of the detectors in order to reduce the costs of thermal cameras dedicated to automotive applications. However, when the pixel size decreases, the depth of field of fast optical system also decreases and reduces the tolerance of the system to optical aberrations. A rule of thumb for evaluating depth of field is to take the largest of the two following equations. The first gives the geometric depth of field and the second gives the diffractive depth of field.

$$geometric\ depth\ of\ field = \pm t_{pix} F\# \qquad (1)$$

$$diffractive\ depth\ of\ field = \pm \lambda F\#^2 \qquad (2)$$

In the case of a design with a F-number (F#) of 1.2 and a detector with a pixel pitch of 10µm (t_{pix}), we obtain a geometric depth of field of ±12µm and a diffractive depth of field of ±14.4µm. In this configuration, the depth of field may therefore not be sufficient to compensate for the Petzval curvature of the optical system. This is particularly problematic for large field of view or medium field of view systems that rely on reverse lens or Petzval design, i.e. optical systems that contain only positive optical powers and for which the Petzval curvature cannot be corrected. The Petzval curvature is given by the following equation:

$$C_p = -\sum_i 1/n_i F_i \qquad (3)$$

C_p is the Petzval curvature, F_i is the focal length of lens number i and n_i is its corresponding index of refraction. So for designs with only positive optical powers, the only way to reduce the Petzval curvature is to increase the index of refraction. High-index Chalcogenide glasses are therefore of great interest and Univ. of Rennes is currently developing TGG [8] and TGS glasses [13] that have an index of refraction greater than 3.

We have designed a reverse lens with a focal length of 5.6mm and a HFOV of 68° as well as a two lens design with a focal length of 8.35mm and a HFOV of 44°. Both designs use a VGA detector with a pixel pitch of 10µm. In 2010, during the EU funded FNIR project (Fusing Far-Infrared and Near-Infrared Imaging for Pedestrian Injury Mitigation), it was determined that, for the automotive application, a minimum F/number (F#) of 1.4 was necessary [14]. In the following, we consider a F/number of 1.2 to take benefit from the small pixel pitch. To focus on geometric aberrations, the designs have been studied at the wavelength of 10µm. Moreover, for both designs, different configurations have been studied.

First, we studied designs with GASIR1, GASIR5 or TGG Chalcogenide glasses.

Then we explored the possibility of further decreasing the Petzval curvature of a design in TGG by replacing the Silicon window of the microbolometers with a Silicon lens. This lens close to the sensor plays the role of a field lens. To maintain a low cost approach, we imposed a constraint on the sag height of the Silicon lens so that it can be realized by

photolithography methods. In a previous work [15], we manage to manufacture a plano-convex Silicon lens with a sag height of 100µm. Another reference reports a sag height of 200µm [16]. In the following, we will consider a maximum sag height of 150µm. We will work as well on plano-concave Silicon lens to ease the lithographic process despite that, in Ref [17], curvatures on both sides of a Silicon lens can be found. In first approximation, the sag height is linked to the radius of curvature *R* and the diameter of the lens ϕ by the following equation:

$$Sag = \frac{\left(\frac{\phi}{2}\right)^2}{2R} \qquad (4)$$

For a plano-convex lens, the focal length is then given by the equation:

$$f = \frac{\left(\frac{\phi}{2}\right)^2}{2(n-1)Sag} \qquad (5)$$

With a sag height of 150µm, a lens diameter of 8mm (diagonal of a VGA sensor with a pixel pitch of 10µm), the focal length of a Silicon plano-concave lens is equal to -22.6mm.

Finally, we explored the potential gain of using curved detectors on a design with either TGG or GASIR1. The benefit of a curved imaging surface was analyzed for mobile camera lenses [18]. The conclusion was that the curved surface allows producing an equivalent lens performing design with faster F-Number than a conventional design. The curved sensor helps achieving uniform image quality over the whole FOV and it increases the effective depth of focus when we consider the full field aberrations. As infrared detectors follow the same trend in terms of decreasing pixel size as cell phone detectors, it is tempting to also evaluate the gain of curved detectors for infrared systems. In a previous work [19], we managed to curve a QVGA detector (320x256 pixels) with a pixel pitch of 25µm. The minimum radius of curvature obtained was equal to 40mm. The sag height obtained is thus equal to 328µm. By reporting this sag height to a VGA sensor with a pixel pitch of 10µm, we could expect a minimum radius of curvature of 24.4mm.

Table 2 analyzes the Petzval curvatures of the reverse lens for different materials based on Eq. 3. With TGG or TGS glasses, the Petzval curvature is lower than with other chalcogenide glasses (GASIR1 and GASIR5). The use of a divergent Silicon lens to replace the window of the IR FPA decreases further the Petzval curvature. The combination of a TGG lens and a Silicon lens gives better results than a Ge lens as shown in the column TGG+Si in Table 2.

Table 2. Evaluation of the Petzval curvature for the reverse lens design

Material	GASIR1	GASIR5	TGS	TGG	Si	Ge	TGG+Si
Index @ 10µm	2.494	2.777	3.12	3.396	3.47	4.004	
C_p (mm^{-1})	-0.072	-0.064	-0.057	-0.053	-0.051	-0.045	-0.039
Sag (mm)	0.573	0.514	0.458	0.421	0.421	0.357	0.316
C_p ZOS (mm^{-1})	-0.059	-0.047		-0.028			-0.022

Figure 2 shows the different configurations for the reverse lens. Figure 3 gives the RMS field maps for these configurations. We notice that the image quality of the optical system is limited by the field curvature and all strategies to reduce it increase the performance of the system: increasing the refractive index of materials, using a field lens or bending the sensor. The best strategy to reduce the Petzval curvature is to bend the sensor. Using a high index of refraction for the lens material reduces the bending of the sensor: the radius of curvature of the sensor with a reverse TGG lens is equal to -45mm whereas the radius of curvature of the sensor with a reverse GASIR1 lens is equal to -14mm. With regard to what has been previously obtained technologically [19], the radius of curvature of the detector with the TGG lens seems to be more easily possible. Nevertheless, the configurations with the TGG lens with or without the Silicon field lens are very efficient solutions with respectively average spot radius RMS values of 7.6µm and 8.4µm, that is to say lower than the pixel size. Finally, we notice that the Petzval curvature of the different reverse lens configurations calculated with the software Zemax Optics Studio (ZOS) are slightly different from the estimated values from Eq. 3. The values calculated with ZOS are given in Table 2. This difference may be explained by the fact that a reverse lens is a thick lens compared to its focal length and that the “divergent” surface is far away from the “convergent” surface allowing to get closer to the properties of a Retrofocus.

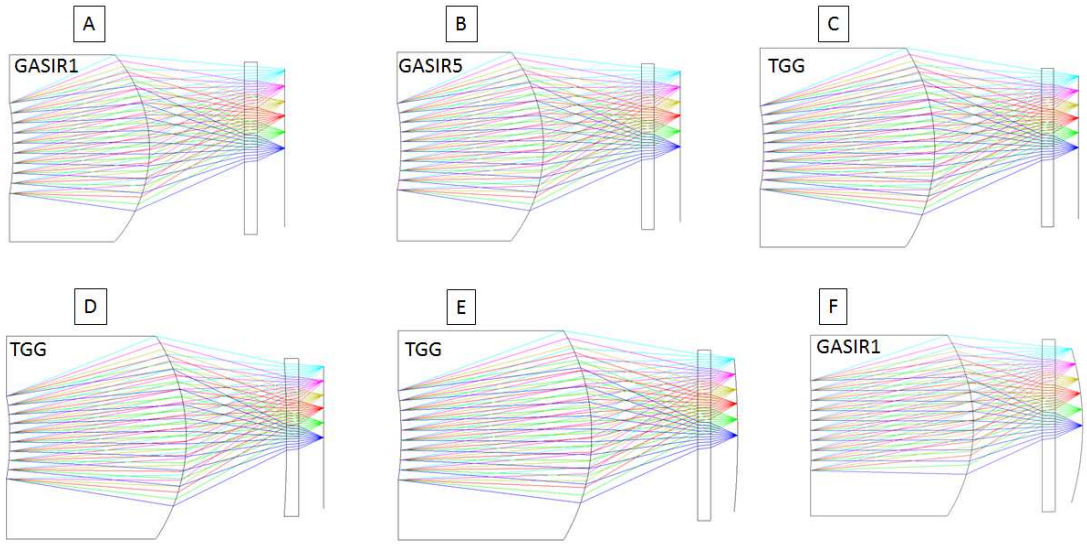

Figure 2. Different configurations of a reverse lens designed for a HFOV of 68° and for a VGA sensor with a pixel pitch of 10µm. A: the material used for the reverse lens is GASIR1. B: the material used for the reverse lens is GASIR5. C: the material used for the reverse lens is TGG. D: the material used for the reverse lens is TGG and we replace the window of the sensor by a divergent Silicon lens. E: the material used for the reverse lens is TGG and the sensor is curved. F: the material used for the reverse lens is GASIR1 and the sensor is curved.

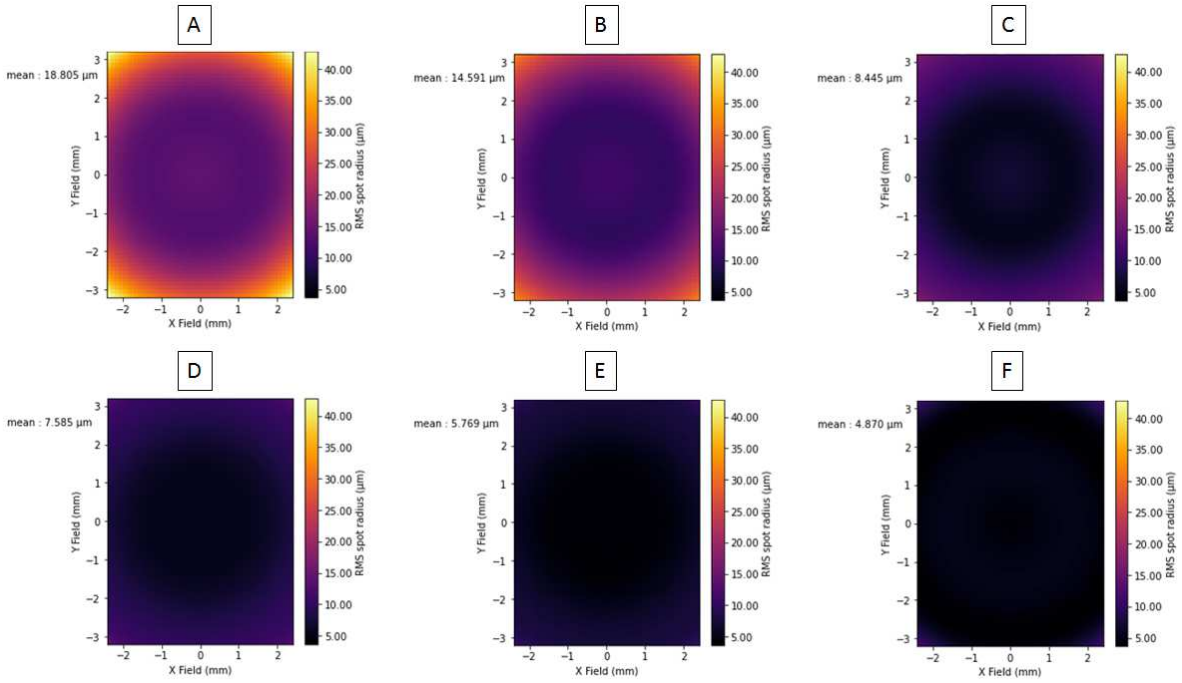

Figure 3. RMS field maps for the different configurations of a reverse lens. A: the material used for the reverse lens is GASIR1. B: the material used for the reverse lens is GASIR5. C: the material used for the reverse lens is TGG. D: the material used for the reverse lens is TGG and we replace the window of the sensor by a divergent Silicon lens. E: the material used for the reverse lens is TGG and the sensor is curved. F: the material used for the reverse lens is GASIR1 and the sensor is curved.

In the case of the two lens design, there exist more configurations. Indeed three types of optical architectures can be designed: Telephoto lens, Petzval lens and Retrofocus lens. Having a divergent optics and a convergent optics, both Telephoto and Retrofocus designs can deal with Petzval curvature which is not the case for the Petzval design which has only convergent optics. For wide field of view system, Petzval design and Retrofocus design are preferred. The advantage of the Petzval design is that the optics can have an aperture smaller than that of the optical system unlike the Retrofocus design where some optics can have an aperture larger than that of the optical system. The choice of one architecture over the other will result from a compromise between the different aberrations. Sometimes it is useful to split an optics into two other optics to reduce their aperture but considering the important cost constraints for automotive applications, we try to do the maximum with only two lenses [20]. In this way, all surfaces are aspherical surfaces up to the 8th order. Like the case of the Reverse lens, we have studied different configurations: lenses in GASIR1, GASIR5 or TGG, the use of a Silicon field lens or a curved sensor. With several options to correct the field curvature and the use of many aspherical surfaces, the merit function has many local minima. We used a global optimizer to find the optimal optical system (Hammer current from ZOS). Finally, we found two families of optical systems according to the allowed footprint.

The first family is a Petzval type design. Figure 4 shows the different configurations of this first family. Figure 5 gives the RMS field maps for these configurations. The gain in performance is not as obvious as in the case of the Reverse lens, but implementing strategies to correct the Petzval curvature can improve the performance of the optical system. The best strategy to reduce the Petzval curvature is to bend the sensor: the design with TGG optics has a sensor with a radius of curvature of -72mm whereas the design with Gasir1 optics has a sensor with a radius of curvature of -28mm. Nevertheless, the configurations with the TGG lens with or without the Silicon field lens are very satisfactory solutions with respectively average spot radius RMS values of 5.0µm and 5.5µm, that is to say lower than the pixel size.

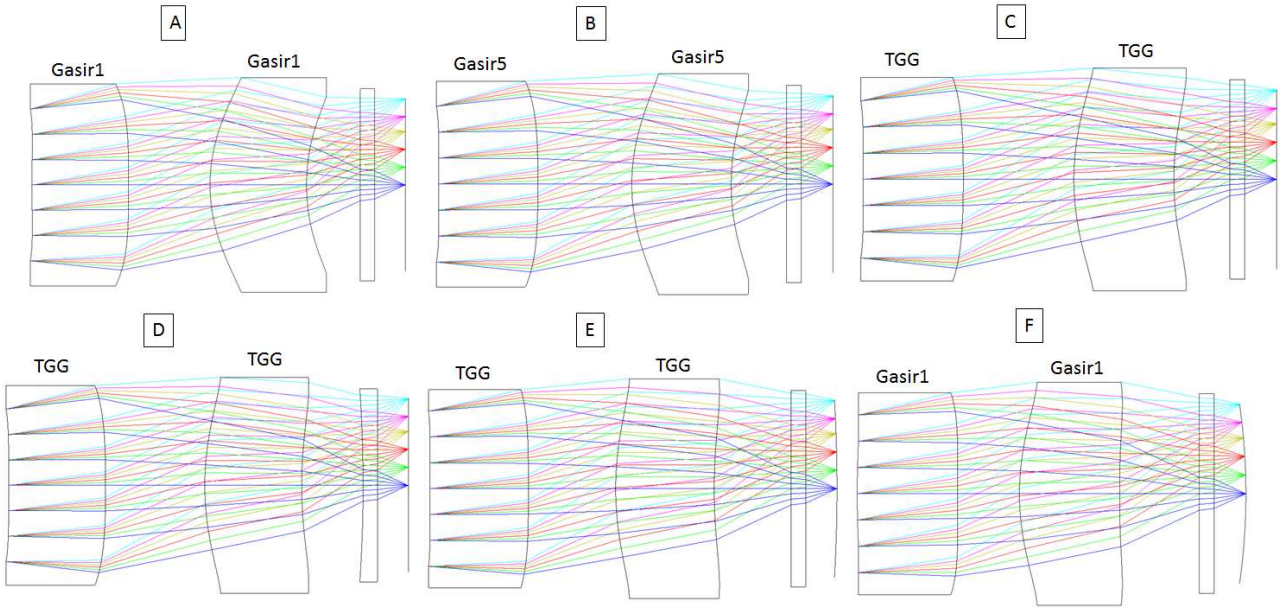

Figure 4. Different configurations of the first two lens design family having a HFOV of 44° for a VGA sensor with a pixel pitch of 10µm. A: the material used for the two lens design is GASIR1. B: the material used for the two lens design is GASIR5. C: the material used for the two lens design is TGG. D: the material used for the two lens design is TGG and we replace the window of the sensor by a divergent Silicon lens. E: the material used for the two lens design is TGG and the sensor is curved. F: the material used for the two lens design is GASIR1 and the sensor is curved.

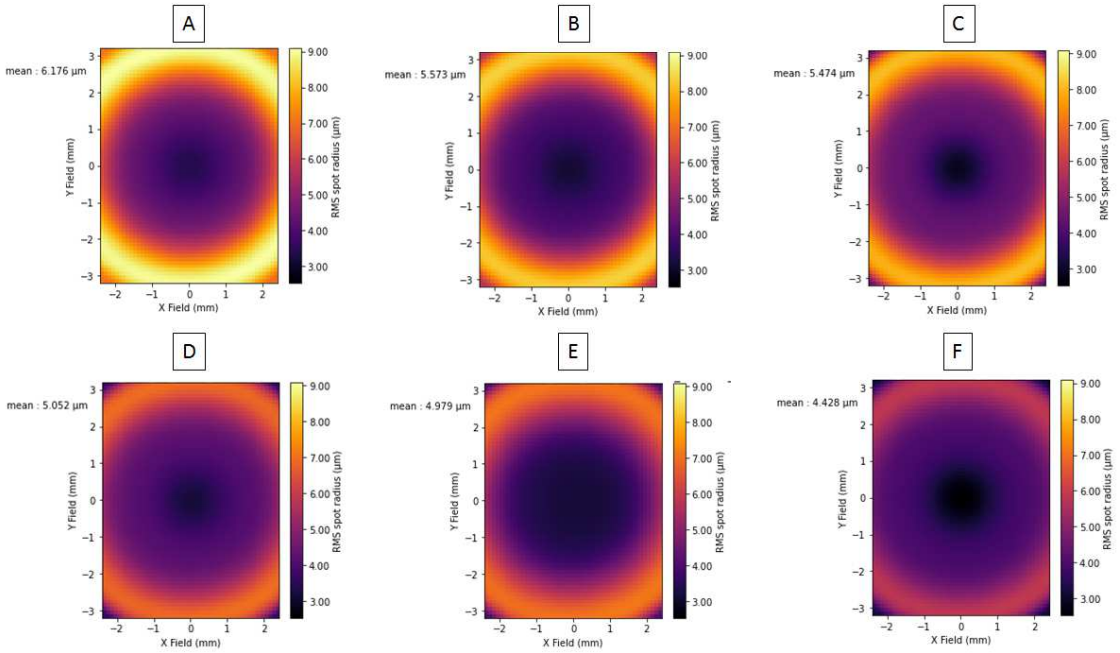

Figure 5. RMS field maps for the different configurations of the first two lens design family. A: the material used for the two lens design is GASIR1. B: the material used for the two lens design is GASIR5. C: the material used for the two lens design is TGG. D: the material used for the two lens design is TGG and we replace the window of the sensor by a divergent Silicon lens. E: the material used for the two lens design is TGG and the sensor is curved. F: the material used for the two lens design is GASIR1 and the sensor is curved.

The second family more compact than the previous one oscillates between a Petzval type design and a Retrofocus type design. Figure 6 shows the different configurations of this second family. Figure 7 gives the RMS field maps for these configurations. Once again, the best strategy to reduce the Petzval curvature is to bend the sensor: the design with TGG optics has a sensor with a radius of curvature of -35mm whereas the design with Gasir1 optics has a sensor with a radius of curvature of -22mm. Nevertheless, the configurations with the TGG lens with or without the silicon field lens are very satisfactory solutions with respectively average spot radius RMS values of 7.7µm and 7.2µm, that is to say lower than the pixel size.

Despite the fact that increasing the refractive index of refraction of the optics improve the performance of the optical system, it is interesting to note that the best results were obtained with GASIR1 optics and a curved sensor. However, the technological feasibility of important curvature of the sensor remains to be demonstrated.

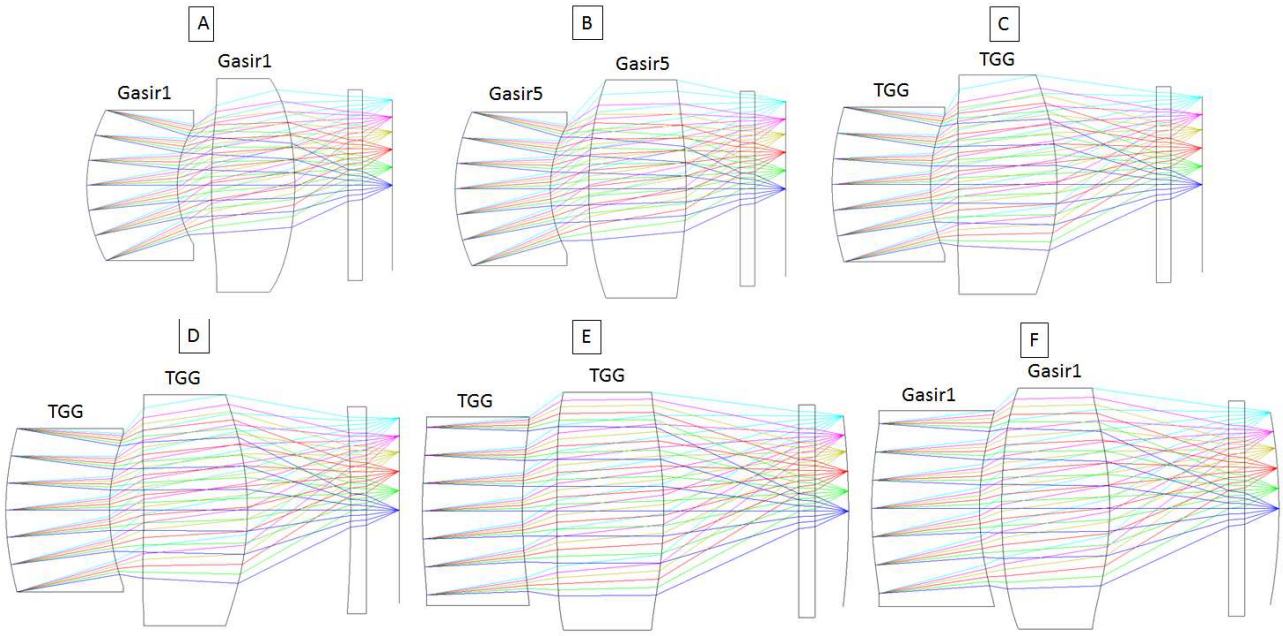

Figure 6. Different configurations of the second two lens design family having a HFOV of 44° for a VGA sensor with a pixel pitch of 10µm. A: the material used for the two lens design is GASIR1. B: the material used for the two lens design is GASIR5. C: the material used for the two lens design is TGG. D: the material used for the two lens design is TGG and we replace the window of the sensor by a divergent Silicon lens. E: the material used for the two lens design is TGG and the sensor is curved. F: the material used for the two lens design is GASIR1 and the sensor is curved.

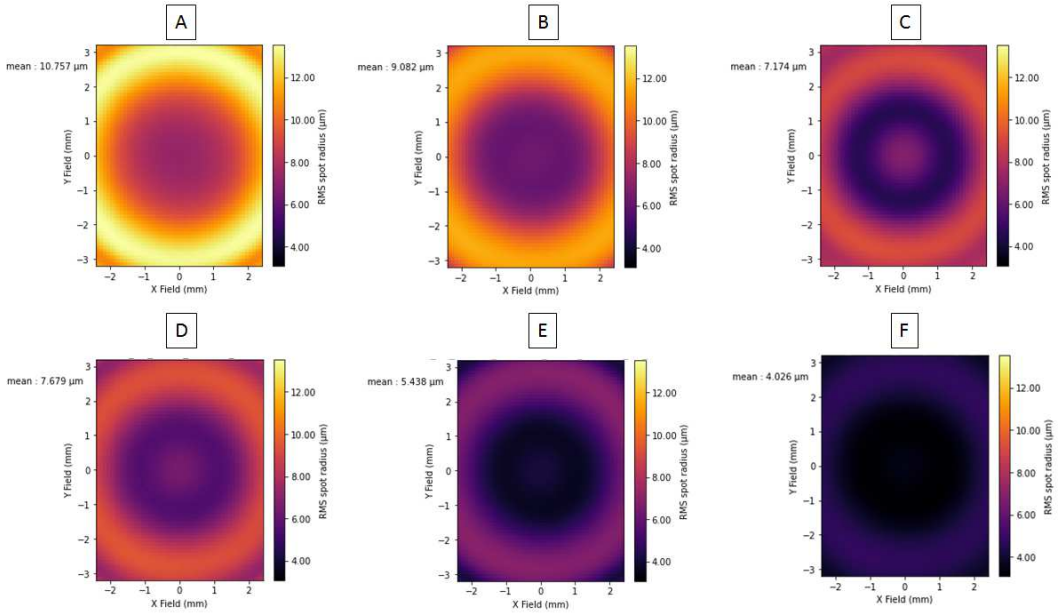

Figure 7. RMS field maps for the different configurations of the second two lens design family. A: the material used for the two lens design is GASIR1. B: the material used for the two lens design is GASIR5. C: the material used for the two lens design is TGG. D: the material used for the two lens design is TGG and we replace the window of the sensor by a divergent Silicon lens. E: the material used for the two lens design is TGG and the sensor is curved. F: the material used for the two lens design is GASIR1 and the sensor is curved.

4. MANUFACTURING AND TEST OF LENSES MADE OF TGG MATERIAL

Two designs were manufactured based on this work. HELIAUS-OPT-82 is a 46° horizontal field of view lens which is a TGG doublet and HELIAUS-OPT-84 is a 69° horizontal field of view lens made of a single TGG lens.

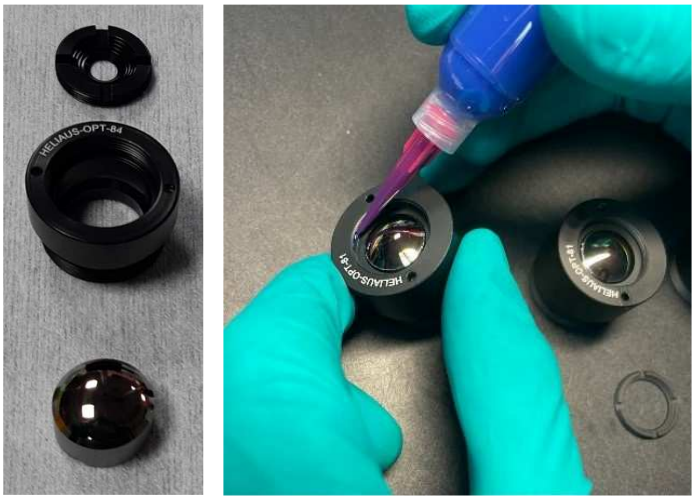

Figure 8. Assembly of lenses. Left: pieces to assemble for lens HELIAUS-OPT-84. Right: final assembly of lens HELIAUS-OPT-82.

Figure 8 displays photographs of the lens assembly process. The lenses are assembled by hand into an aluminium housing. On the left hand side, one can see the different pieces which constitute the assembly of lens HELIAUS-OPT-84. This lens is a TGG singlet which is simple to assemble with a lens barrel and a clamp ring to secure it in place. On the right hand side, an operator is finishing the assembly of lens HELIAUS-OPT-82, which is another Heliaus prototype lens. The mounting principle is the same for all lenses. On the photograph, the operator is applying thread lock to secure the front lens clamp ring in place.

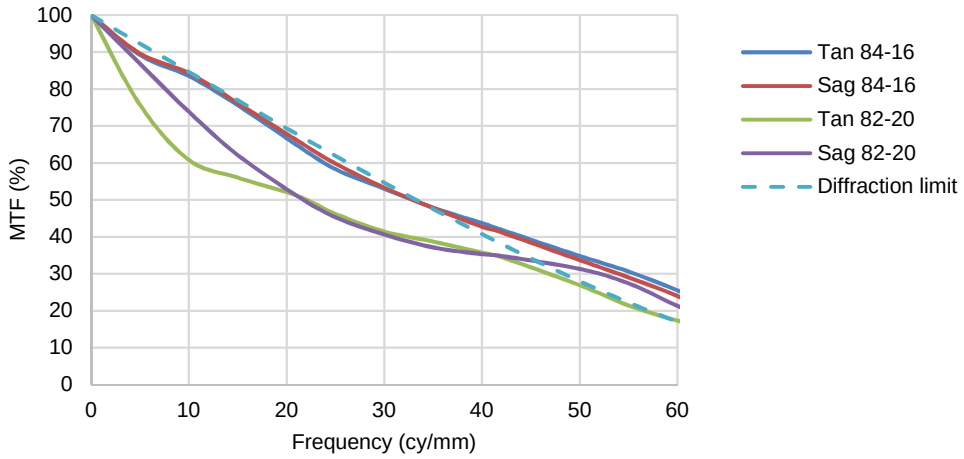

Figure 9. Measurement of MTF on axis for lenses 82-20 and 84-16.

Figure 9 shows the measurement of the Modulation Transfer Function (MTF) for two prototype lenses (HELIAUS-OPT-82, serial number 20 and HELIAUS-OPT-84, serial number 16). The value of the MTF is displayed as a function of the spatial frequency up to 60 cy/mm. The diffraction limit for an f/1.2 aperture is also displayed. One can notice some

measurement curves go above the diffraction limit for frequencies higher than 40 cy/mm. This is attributed to measurement bench inaccuracy at these high spatial frequencies. For lens 84-16, the MTF follows the diffraction limit closely, demonstrating exceptional performance. For lens 82-20, on the other hand, the MTF is a bit lower. This can be explained by the fact that lens 82 is a doublet lens that is subject to more tolerance stacking and can be expected to have a slightly lower performance. This being said, the lens behaves exceptionally well by remaining close to the diffraction limit.

These measurements validate the use of TGG in lens design as an excellent material. However, managing to produce this glass in large quantities for industrial processes and applications remains a challenge.

5. CONCLUSION

IR FPA with small pixel pitch seem to be key technologies to meet the cost requirement of automotive industry. However, the reduction of the pixel pitch represents an important challenge for the optical designer to maintain the optical performance with a minimum number of lenses. It is indeed important to limit the number of optics to reduce the cost of the system. Using higher index materials is one way to reconcile simplicity of the optical architecture with performance. For small-size optics, the final cost of IR optics is mainly governed by the synthesis and processing instead of raw materials. We also explored the possibility of replacing the microbolometer window with a divergent field lens or of using a curved detector. Both approaches will however increase the cost of the detector. Finally, we made the choice in this paper to limit the aperture to F/1.2. However, such an aperture associated with small pixels remains to be evaluated experimentally in real driving condition.

ACKNOWLEDGMENT

This research is supported and funded by the Heliaus European Union Project. The project focused on enabling safe autonomous driving systems. This project has received funding from the ECSEL Joint Undertaking (JU) under grant agreement No 826131. The JU receives support from the European Union's Horizon 2020 research and innovation program and France, Germany, Ireland, Italy.

REFERENCES

[1] Sebastien Becker, Pierre Imperinetti, Jean-Jacques Yon, Jean-Louis Ouvrier-Buffet, Valérie Goudon, Antoine Hamelin, Claire Vialle, Agnès Arnaud, "Latest pixel size reduction of uncooled IR-FPA at CEA, LETI," Proc. SPIE 8541, Electro-Optical and Infrared Systems: Technology and Applications IX, 85410C (24 October 2012)

[2] https://sierraolympic.com/thermal-imaging-articles/company-news/introducing-ten%C2%B5m-the-smallest-pixel-pitch-lwir-camera-on-the-market/

[3] Christian Vieider, Stanley Wissmar, Per Ericsson, Urban Halldin, Frank Niklaus, Göran Stemme, Jan-Erik Källhammer, Håkan Pettersson, Dick Eriksson, Henrik Jakobsen, Terje Kvisterøy, John Franks, Jan VanNylen, Hans Vercammen, Annick VanHulsel, "Low-cost far infrared bolometer camera for automotive use," Proc. SPIE 6542, Infrared Technology and Applications XXXIII, 65421L (14 May 2007)

[4] Arnaud Crastes, Jean-Luc Tissot, Yann M. Guimond, Pier Claudio Antonello, Joel Leleve, Hans-Joachim Lenz, Pierre Potet, Jean-Jacques Yon, "Low cost uncooled IRFPA and molded IR lenses for enhanced driver vision," Proc. SPIE 5251, Detectors and Associated Signal Processing, (19 February 2004)

[5] Valldorf, Jürgen, and Wolfgang Gessner, éd. « Far Infrared Low-Cost Uncooled Bolometer for Automotive Use ». In Advanced Microsystems for Automotive Applications 2007, 265-78. Berlin, Heidelberg: Springer Berlin Heidelberg, 2007.

[6] A. Novikova, "Élaboration d'optiques infrarouges par combinaison de la mécanosynthèse et du frittage SPS," thesis, Rennes 1 (2018).

[7] H. G. Dantanarayana, N. Abdel-Moneim, Z. Tang, L. Sojka, S. Sujecki, D. Furniss, A. B. Seddon, I. Kubat, O. Bang, and T. M. Benson, "Refractive index dispersion of chalcogenide glasses for ultra-high numerical-aperture fiber for mid-infrared supercontinuum generation," Opt. Mater. Express 4(7), 1444–1455 (2014).

[8] S. Zhang, X. Zhang, M. Barillot, L. Calvez, C. Boussard, B. Bureau, J. Lucas, V. Kirschner, and G. Parent, “Purification of Te75Ga10Ge15 glass for far infrared transmitting optics for space application,” Opt. Mater. 32(9), 1055–1059 (2010).
[9] S. Maurugeon, C. Boussard-Pledel, J. Troles, A. J. Faber, P. Lucas, X. H. Zhang, J. Lucas, and B. Bureau, “Telluride Glass Step Index Fiber for the far Infrared,” J. Lightwave Technol. 28(23), 3358–3363 (2010).
[10] S. Maurugeon, B. Bureau, C. Boussard-Plédel, A. J. Faber, X. H. Zhang, W. Geliesen, and J. Lucas, “Te-rich Ge–Te–Se glass for the CO2 infrared detection at 15μm,” J. Non-Cryst. Solids 355(37-42), 2074–2078 (2009).
[11] D. J. Sarrach, J. P. De Neufville, and W. L. Haworth, “Studies of amorphous GeSeTe alloys (I): Preparation and calorimetric observations,” J. Non-Cryst. Solids 22(2), 245–267 (1976).
[12] X. Peng, L. Jiang, G. Li, Y. Yuan, Y. Wang, S. Dai, N. Zhang, J. Su, P. Yang, and P. Zhang, “Fabrication and characterization of multimaterial Ge25Se10Te64/As2S3 chalcogenide fiber with a high value of the numerical aperture,” J. Non-Cryst. Solids 525, 119690 (2019).
[13] V. Reux, L. Calvez, S. Billon, A. Gautier, H. Ma, P. Houizot, F. Charpentier, H. Tariel, Z. Yang, A. Yang, and X.-H. Zhang, "High refractive index IR lenses based on chalcogenide glasses molded by spark plasma sintering," Opt. Mater. Express 11, 1622-1630 (2021)
[14] R. Schweiger, S. Franz, O. Loehlein, W. Ritter, Franks J and T. Krekels, "Sensor fusion to enable next generation low cost Night Vision systems," in Proc. SPIE 7726, Optical Sensing and Detection, 772610 (May 13, 2010); doi:10.1117/12.855932, Brussels, 2010.
[15] Florence de la Barrière, Guillaume Druart, Nicolas Guérineau, Gilles Lasfargues, Manuel Fendler, Nicolas Lhermet, and Jean Taboury, "Compact infrared cryogenic wafer-level camera: design and experimental validation," Appl. Opt. 51, 1049-1060 (2012)
[16] Eric Logean, Lubos Hvozdara, Joab Di-Francesco, Hans Peter Herzig, Reinhard Voelkel, Martin Eisner, Pierre-Yves Baroni, Michel Rochat, Antoine Müller, “High numerical aperture silicon collimating lens for mid-infrared quantum cascade lasers manufactured using wafer-level techniques,” Proc. SPIE 8550, Optical Systems Design 2012, 85500Q (December 18, 2012), doi:10.1117/12.981165.
[17] David Ovrutsky, Jeremy Huddleston, Paul Elliott, David Keller, Richard Jones, Thomas Mercier, TIR imaging lens image capturing system having the same and associated methods US20150109456
[18] Dmitry Reshidko and Jose Sasian, "Optical analysis of miniature lenses with curved imaging surfaces," Appl. Opt. 54, E216-E223 (2015)
[19] Delphine Dumas, Manuel Fendler, Frédéric Berger, Baptiste Cloix, Cyrille Pornin, Nicolas Baier, Guillaume Druart, Jérôme Primot, and Etienne le Coarer, "Infrared camera based on a curved retina," Opt. Lett. 37, 653-655 (2012)
[20] Chris Bigwood, Andrew Wood, "It's only two lenses in a tube: how complicated can it be?," Proc. SPIE 7298, Infrared Technology and Applications XXXV, 72980Z (6 May 2009)